

Microscopic Examination of Nanosized Mixed Ni#Al Hydroxide Surface Precipitates on Pyrophyllite

Kenneth J. T. Livi, Giorgio S. Senesi, Andreas C. Scheinost, and Donald L. Sparks

Environ. Sci. Technol., **2009**, 43 (5), 1299-1304 • DOI: 10.1021/es8015606 • Publication Date (Web): 12 January 2009

Downloaded from <http://pubs.acs.org> on March 23, 2009

More About This Article

Additional resources and features associated with this article are available within the HTML version:

- Supporting Information
- Access to high resolution figures
- Links to articles and content related to this article
- Copyright permission to reproduce figures and/or text from this article

[View the Full Text HTML](#)



Microscopic Examination of Nanosized Mixed Ni–Al Hydroxide Surface Precipitates on Pyrophyllite

KENNETH J. T. LIVI,^{*,†}
GIORGIO S. SENESI,^{‡,§}
ANDREAS C. SCHEINOST,^{||} AND
DONALD L. SPARKS[‡]

Department of Earth and Planetary Sciences, Johns Hopkins University, Baltimore, Maryland 21218, Department of Plant and Soil Sciences and Center for Critical Zone Research, University of Delaware, Newark, Delaware 19717-1303, CNR-IMIP Istituto di Metodologie Inorganiche e dei Plasmi, Via Amendola, 122/D - 70126 Bari, Italy, Molecular Structures Group, Institute of Radiochemistry, FZD, Dresden, Germany, and Rossendorf Beamline at ESRF, 38043 Grenoble, France

Received June 6, 2008. Revised manuscript received December 3, 2008. Accepted December 5, 2008.

The nature of Ni-hydroxide precipitates on pyrophyllite were re-examined by analytical electron microscopy (AEM), high-resolution transmission electron microscopy (HRTEM), selected-area electron diffraction (SAED), powder X-ray diffraction (PXRD), and extended X-ray absorption fine structure (EXAFS) spectroscopy. Chemical analysis of precipitates showed that the precipitate contains about 20% Al. HRTEM imaging showed that the precipitate was amorphous and PXRD failed to find any crystalline peaks associated with crystalline Ni–Al layered double-hydroxide (LDH) or α -Ni(OH)₂. These results confirmed the conclusion from EXAFS spectroscopic data that Al coprecipitated with Ni on Al-rich substrates to form Ni–Al LDH surface precipitates. However, the HRTEM data clarifies that although the bonding environment of the precipitate is like that of Ni–Al LDH, no long-range ordering of the structure exists. The study illustrates the need for TEM observations to complement EXAFS data and the potential importance of amorphous materials in environmental settings.

Introduction

Sorption of heavy metals on soil and sediment components such as clay minerals, metal oxides, and organic matter is a major process controlling the fate and transport of metals in the environment. A number of studies have shown that metal hydroxide and mixed-metal hydroxide precipitates can form on the surfaces of clay minerals, metal oxides, and on soils (1–8). The role that surface precipitates and coprecipitates play in toxic element attenuation and release has gained considerable attention. Mixed metal–Al hydroxide (Co–Al, Ni–Al, and Zn–Al) precipitates can form on soil mineral surfaces and in contaminated soils (3–7). These precipitates form at pH values below the thermodynamic

solubility product of crystalline minerals, at below monolayer coverages, and, in some cases, on time scales of minutes (3, 5, 6). The short-range order of these precipitates is similar to that of crystalline layered double hydroxides (LDH), characterized by brucite octahedral sheets, in which trivalent Al substitutes for divalent metal cations (Co, Ni, Zn), and the net positive charge in the octahedral layer is satisfied by anions, such as nitrate, silicate, and carbonate, in the interlayer position. Over time, the mixed metal–Al hydroxides are transformed into a precursor metal phyllosilicate phase, which greatly sequesters the metal, significantly inhibiting metal release and diminishing bioavailability (9–11). The mechanism for the metal sequestration is due to increased silication of the interlayer phase. Direct thermodynamic measurements (enthalpies of formation) have recently shown that LDHs that have silicate interlayers are much more stable than those dominated by nitrate and sulfate (12).

A number of studies have shown that in soils Zn- and Ni-LDH phases formed and, even at low pH (4), metal release was significantly retarded (1–4). Recently, Grafe et al. (13) have shown, using microfocused X-ray fluorescence and EXAFS spectroscopy, that mixed metal arsenate precipitates are major species in copper-chromated-arsenate contaminated soils.

Experimental studies of Ni surface precipitates have included a number of characterization methods to describe the nature of the precipitates produced in experiments. Most studies have employed EXAFS spectroscopy that indicate that the Ni–Ni bond distances were consistent with a Ni hydroxide type precipitate (15) and references therein). The use of differential diffuse reflectance spectroscopy (DRS) added the conclusive evidence that Al was coprecipitating with Ni (14) and the precipitate was a mixed Ni–Al hydroxide precipitate of the takovite form. Aluminum was derived from partial dissolution of pyrophyllite.

In addition to EXAFS, a TEM study was undertaken by Scheidegger et al. (15) to visualize the precipitates on pyrophyllite. Surface deposits, not present on non-Ni treated pyrophyllite, were found. At low Ni sorption densities, surface precipitation seemed to occur preferentially along the edges of pyrophyllite. However, compared to today's capabilities, the microscopes used provided limited HRTEM resolution. It was therefore possible that crystalline material could be present in small amounts, but not identified as such through imaging. No SAED results were presented to identify the crystalline form of the precipitate.

The present study was initiated to more carefully characterize the crystalline nature of the Ni hydroxide precipitates, and over a longer reaction period than previous studies (5 years). XRD patterns were taken of starting materials, various reacted products (different residence times), and standard material of several Ni-hydroxides. The data were complemented with EXAFS analysis of a five year Ni-reacted pyrophyllite sample. The current study used a TEM with sufficient imaging resolution (better than 0.2 nm) to determine the degree and distribution of crystallinity of the precipitates. SAED patterns were examined to determine if crystalline Ni-hydroxides exist. In addition, careful AEM analyses were made to determine the precipitate composition.

Experimental Section

Sample Preparation. The pyrophyllite used in the study came from Robbins, NC and was fractionated and reacted with Ni as described in Scheidegger et al. (15). After fractionation, the pyrophyllite was saturated with Na by washing three times with 0.5 M NaNO₃, then resuspended with distilled

* Corresponding author phone: 410-516-8342; fax: 410-516-7933; e-mail: klivi@jhu.edu.

[†] Johns Hopkins University.

[‡] University of Delaware.

[§] CNR-IMIP Istituto di Metodologie Inorganiche e dei Plasmi.

^{||} Institute of Radiochemistry, FZD and Rossendorf Beamline at ESRF.

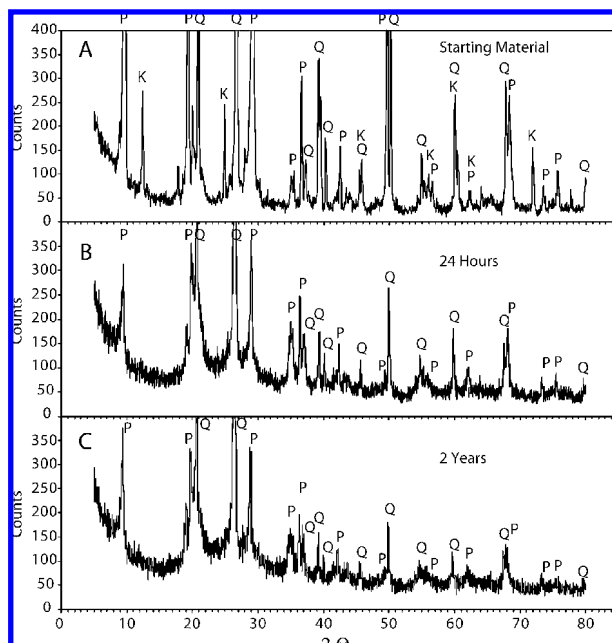


FIGURE 1. Powder X-ray diffraction profiles of the uncoated pyrophyllite (A) and reaction durations of 24 h (B) and 2 yr (C). P = pyrophyllite, K = kaolinite, Q = quartz.

water and centrifuged. The clear supernatant was discarded and excess salts were removed by dialysis until the electrical conductivity of the equilibrium solution was <10 uS/cm. Thereafter, the white clay material was freeze-dried. Nickel sorption samples were prepared using a batch technique designed to maintain constant pH (pH stat) and temperature (298 K) and to eliminate CO_2 by purging with N_2 . The pyrophyllite was hydrated in a 0.1 M NaNO_3 solution for 24 h prior to reaction with Ni. After hydration the pH of the suspension was adjusted to pH 7.5 with 0.1 M NaOH and the mixture was brought to a solid/liquid ratio of 10 g/L. Ni from a 0.1 M $\text{Ni}(\text{NO}_3)_2$ stock solution was dispensed in stepwise additions (within 5 min) to avoid formation of Ni precipitates due to local oversaturation of the suspension. The pH was automatically held constant (pH 7.5) and the electrode was recalibrated every 24 h. The initial Ni concentration (3 mM) and the reaction pH (7.5) were selected to achieve considerable sorption densities and to ensure that the bulk solutions were undersaturated with respect to crystalline $\text{Ni}(\text{OH})_3$. Reaction times of 1 h, 24 h, and 1, 2, and 5 years were studied.

X-ray Diffraction. X-ray diffraction patterns of oriented mounts (simple dispersion of grains on a glass slide) were obtained with a Philips XRG 3100 powder diffractometer using $\text{Cu K}\alpha$ radiation. Scans were made over a variety of 2θ ranges, counting times, and step sizes each designed to search for relevant peaks or to characterize the starting material.

EXAFS Spectroscopy. Ni K-edge EXAFS spectra were collected at the Rossendorf Beamline at ESRF (Grenoble, France) on the 5-year reaction run at 15 K. This allows for the comparison of an extremely long run with previously published data. The results are given in the Supporting Information.

TEM. Small quantities of powdered reactants were dispersed in deionized water and ultrasonicated for 3 min. A 200-mesh Cu grid with a lacey-carbon support film was dipped into the suspension and dried. TEM analyses were made using a Philips CM 300 FEG microscope equipped with an Oxford light element energy dispersive X-ray spectroscopy (EDS) detector and a Gatan GIF 200 CCD imaging system. The point-to-point resolution of the TEM is less than 0.2 nm and the line resolution is 0.09 nm. Images were analyzed and processed using the Gatan Digital Micrograph v. 3.0 software.

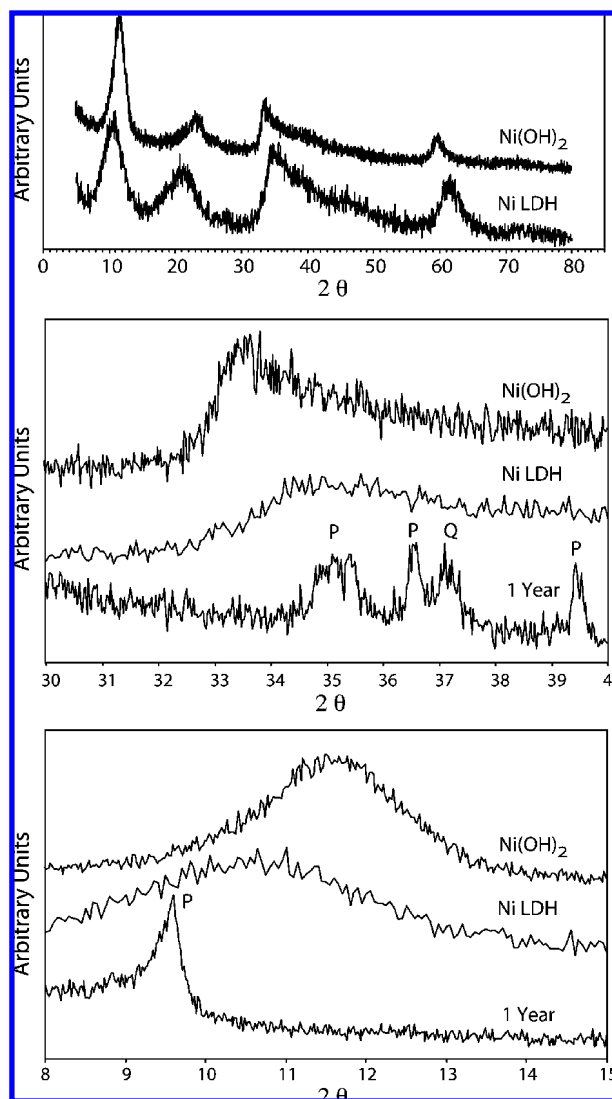


FIGURE 2. Full range powder X-ray diffraction scans of synthetic Al-free Ni LDH and α - $\text{Ni}(\text{OH})_2$ (top). Scans are vertically offset for clarity. Comparison of selected regions where Ni LDH and α - $\text{Ni}(\text{OH})_2$ should appear if present (middle and bottom). No amorphous humps were found at the angles where Ni LDH and α - $\text{Ni}(\text{OH})_2$ are (11 – 12° and 33° 2θ).

The software package ES Vision4 was used to process EDS spectra. SAED patterns were digitized and processed by Digital Micrograph software and circularly averaged by the program LISPIX (16).

Results

XRD. Unreacted pyrophyllite XRD patterns are shown in Figure 1a. It contains predominantly pyrophyllite with minor amounts of quartz and kaolinite. Although the peaks are consistent with pyrophyllite, random mounts are preferred for identification of the polytype (1Tc, 2M). Scheidegger et al. (15) reported that there was a small amount of quartz ($<5\%$) present, but did not find kaolinite. The fact that we found kaolinite indicates that some heterogeneity in the starting material exists, or that preferred orientation effects in sedimented samples masked the presence of kaolinite in the earlier studies.

Nickel-reacted pyrophyllite XRD patterns of the 24-h and 2-yr reacted pyrophyllite are given in Figure 1b and c. The 0.7 nm peak for kaolinite ($\sim 12^\circ$ 2θ) is absent after 24 h, but quartz peaks remain even in the 2-yr run, although there is a reduction in their intensity. For the 24-h run, there is an

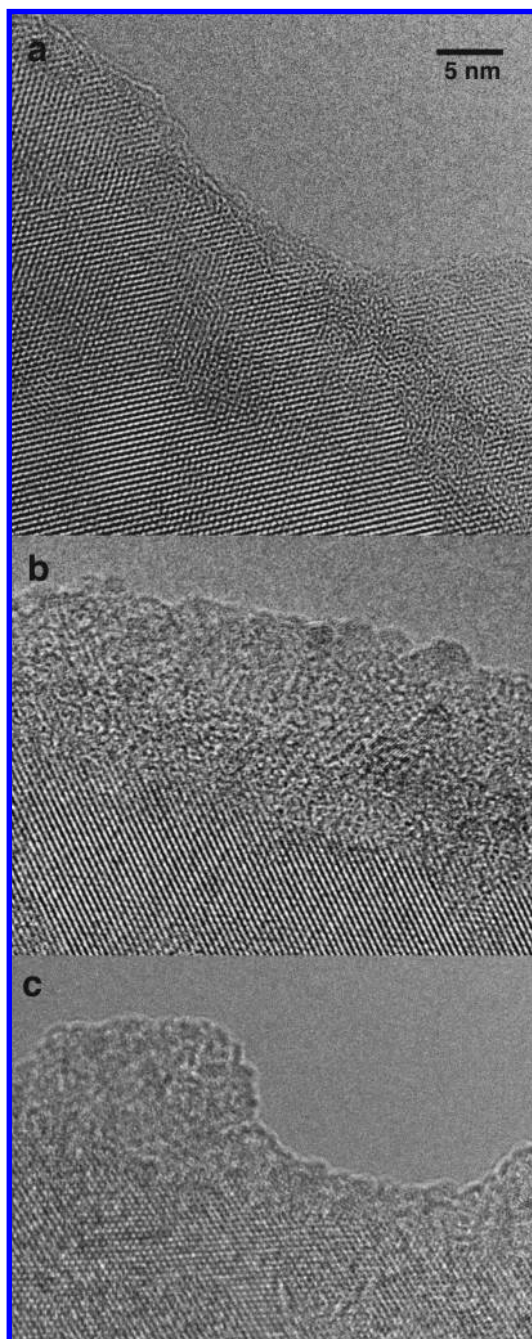


FIGURE 3. HRTEM images looking down the c^* axis of (a) starting pyrophyllite, (b) 24-h, and (c) 5-yr run.

increase in the background in the range of $20\text{--}30^\circ 2\theta$. This hump in the background increases in the 2-yr run.

In Figure 2a, XRD patterns for synthetic Ni–Al LDH and α -Ni(OH)₂ are presented. These patterns show a lack of sharp peaks which is typical of nanometer-sized particles of metal-hydroxides. In comparing these synthetic specimens, the sharper peaks of the α -Ni(OH)₂ sample indicate a greater degree of ordering and/or crystal size. The reference material is compared to the 1-yr Ni-reacted pyrophyllite in two sets of slow scans (Figure 2b and c). No evidence of either reference material can be found in the regions between $8\text{--}15^\circ$ and $30\text{--}40^\circ 2\theta$.

EXAFS. The EXAFS spectrum of pyrophyllite reacted with Ni for 5 years is shown in Figure S1. A characteristic structural feature of Ni,Al-LDH ((Ni,Al)₃(OH)₆) in comparison to Ni hydroxides is the presence of both Ni and Al atoms in the first metal shell at a relatively short distance of 3.06 Å, which

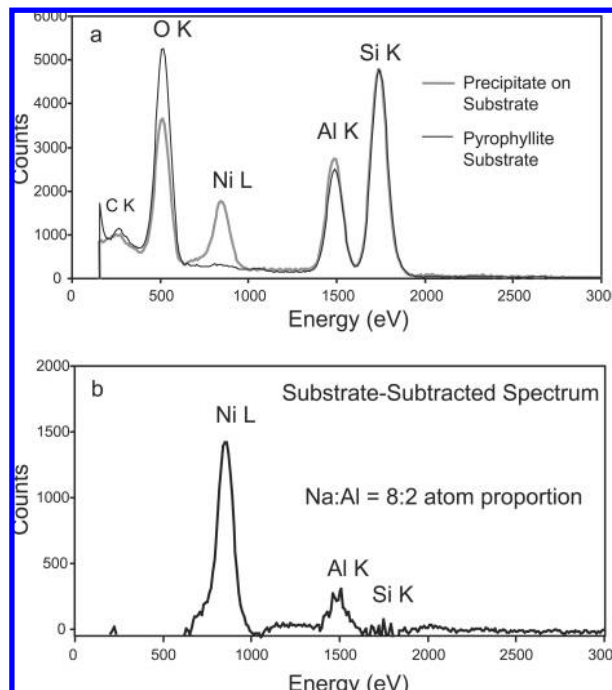


FIGURE 4. (a) Summation of 15 edge EDS analyses of precipitate and pyrophyllite substrate. (b) After subtraction of substrate from edge analyses (5-yr sample) normalized to Si intensity.

is difficult to ascertain by shell fitting. However, the destructive interference of Ni and Al backscattering waves produces a characteristic beat pattern at about 8 \AA^{-1} , which can be used as a fingerprint for LDH (see arrow in Figure S1b) (17). Wavelet analysis of the combined k -space and r -space dependency of the $2.6\text{-\AA} + \Delta R$ FT peak also indicates the presence of a lighter (Al) and a heavier (Ni) backscattering atom at this distance (Figure S1c) (18). In conclusion, all spectral features are consistent with LDH, and a good fit of the experimental spectra was obtained by accounting for the theoretical structure of LDH.

The metal coordination numbers are consistently smaller than the expected values. This points to a substantial structural disorder or limited particle size in the range of a few nanometers, in line with the EM results. The Al/Ni atomic ratio observed for the first metal shell is $0.5/3.7 = 0.14$ (error range $0.08\text{--}0.23$ based on a 25% error of coordination numbers). Assuming that 1/3 of all metal centers are occupied by trivalent Al (limited by charge distribution), the first shell should contain equal amounts of Ni and Al, hence this ratio would be 1. Therefore, the Al content of the observed LDH phase falls significantly below this maximum value, again in line with EM.

HRTEM. The starting pyrophyllite material was examined in the TEM as a control for further examinations. A small and variable amount of amorphous material was found at the edge of the unreacted pyrophyllite crystals (Figure 3a). This is commonly found in TEM observations and can be due to three processes: (1) The electron beam acts as a getter for carbon during sample exposure creating self-contamination deposits from carbon derived from the holey-carbon support film or from organic matter within the interlayer. (2) Beam damage and amorphization of pyrophyllite starts as soon as the sample is exposed to the beam. Amorphization nucleates at the edge of the particles and progresses inward. And (3) Reaction of pyrophyllite with distilled water. These processes make it difficult to know if there was an original amorphous layer on the pyrophyllite before examination in the TEM. However, the amount of amorphous material is much less

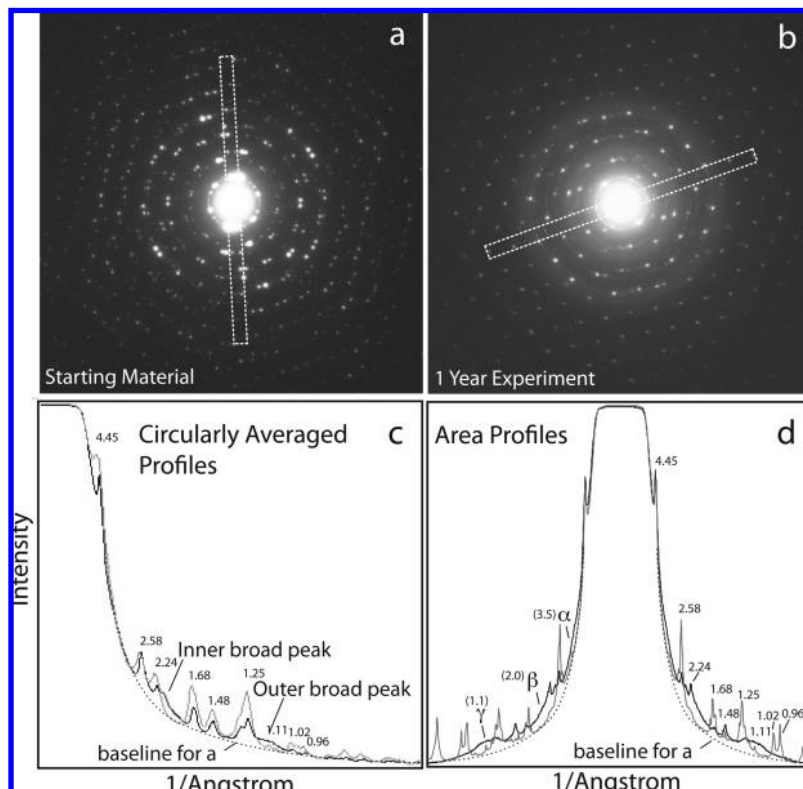


FIGURE 5. SAED patterns for the starting material (a) and 1-yr run (b). (c) Circularly averaged profiles for (a) (light curve) and (b) (dark curve). (d) Profiles of rectangular areas drawn in (a) (light curve) and (b) (dark curve). Peaks are labeled in Å⁻¹.

than what was observed in Ni-reacted samples. AEM analyses of the starting material yield spectra consistent with pyrophyllite. There was no evidence of Ni in the starting material and the pyrophyllite contained only minor amounts of K.

HRTEM images of the 24-h and 5-yr Ni-reacted pyrophyllite samples are shown in Figure 3b and c. All samples show evidence of the addition of amorphous material to the pyrophyllite crystals. Care was taken to determine if beam exposure created the amorphous material. Although the amount of amorphous material would apparently increase with beam exposure (see Supporting Information), even with the greatest care taken, initial observations showed that there was amorphous material present and was not due to beam damage. Based on a number of TEM observations (several tens of micrographs for each sample sited in this study), there was no correlation between the thickness of the amorphous layers and reaction duration.

Beam Damage Study. During the course of HRTEM observations, long-term beam exposure altered the material in three ways: (1) the crystalline pyrophyllite became amorphous and the boundary between the precipitate and the pyrophyllite became indistinct; (2) there was mass-loss of material; and (3) within the Ni-rich amorphous precipitate, small crystallites nucleated. A time-lapse series of HRTEM images is shown in Figure S2, where all three processes can be seen—the pyrophyllite lattice fringes disappear, the edge of the crystal recedes, and lattice fringes of another phase appear at the edge of the crystal. Analysis of the layer spacings of HRTEM images and SAED patterns indicate that these crystals have the bunsenite structure (NiO₂). Thus, extended beam exposure dehydrates the precipitates. Beam-induced dehydration has also been reported for brucite (Mg(OH)₂) which transforms to nanocrystalline periclase (MgO) (19).

AEM. AEM analyses indicate that Ni is present on all surfaces ($\{hk0\}$ and $\{00l\}$) of pyrophyllite. During the course of AEM analysis, it was determined that there was a progressive loss of Al from the precipitate during analyses with relatively high electron flux. The precipitate thin film

covering the pyrophyllite substrate necessitates analyses using a finely focused beam (around 10 nm). Certain procedures were taken in order to avoid Al loss during analysis: (1) elongating the beam parallel to the edge of the grain (reducing the electron flux while maintaining the current and spatial resolution in one direction), (2) keeping the analysis time short (50 s), and (3) summing many analyses to improve precision.

The summed spectrum of 15 edge analyses from the 5 yr sample was compared to the average analysis ($n = 7$) for the pyrophyllite starting material in Figure 4a. Notice that the edge analyses also include Si from pyrophyllite. All analyses of the precipitate included some portion of the substrate. It was assumed that Si was only present in pyrophyllite and that pyrophyllite has a fixed Al:Si ratio of 1.92(0.08 2σ). The two spectra have been normalized to their Si peaks. Stripping the pyrophyllite analysis from the precipitate resulted in the residual in Figure 4b. Quantitative decomposition of this residual results in a Ni:Al atomic ratio of 80.5(8.5):19.5(2.0) or 0.24(0.03). This is within error of the EXAFS estimate.

On the basis of the LDH model with a neutral octahedral layer, the mineral formula (rounded to the nearest tenth atom) would be (Ni_{2.2}Al_{0.5}□_{0.3})(OH)₆, where □ denotes vacancies in the octahedral layer. This is an example of a dioctahedral-trioctahedral substitution that is relatively rare in clay minerals. If vacancies are not present to maintain a neutral layer, then an interlayer species must be included to balance charges and the mineral formula would be (Ni_{2.4}Al_{0.6})IC_{0.6}(OH)₆, where IC represents a monovalent interlayer species.

SAED. SAED patterns for unreacted and reacted pyrophyllite were obtained to confirm the amorphous nature of the precipitate and are presented in Figure 5a and b. In both patterns, the only sharp reflections present were for pyrophyllite. In addition to these reflections, diffuse rings were found. Since the SAED patterns were taken from crystals extending into holes within the carbon support film, these rings are not due to the holey-C support film. The SAED

patterns in Figure 5a and b were circularly averaged and plotted in Figure 5c. In addition, area profiles were generated from sectors in each pattern that minimizes the contribution of the pyrophyllite reflections while maximizing the amorphous intensity. The unreacted material does not contain significant amorphous material and therefore, no diffuse rings are present. In comparison, the 1-year SAED profiles contain intensity not associated with Bragg diffraction of pyrophyllite. These amorphous rings are labeled as α , β , and γ in Figure 5d. The approximate centroids for these bands are 3.5, 2.0, and 1.1 Å, respectively.

Discussion

The HRTEM images clearly identify the precipitate on pyrophyllite as amorphous. The SAED patterns contain diffuse scattering consistent with amorphous material with real spacings of 3.5, 2.0, and 1.1 Å. The interatomic distances of Ni–Ni and Ni–Al in Ni–Al LDH are on the order of 3.06 Å (2) which is shorter than the α ring. The presence of amorphous carbon deposited during exposure to the electron beam cannot be ruled out and may contribute to the shift of the band to larger d -spacings (amorphous C has a ring at 3.4 Å). The β ring is close to the Ni–O distance of 2.05 Å. However, since these peaks are broad, they do not precisely clarify the actual structure of the amorphous material.

Scheinost et al. (14) reviewed the EXAFS data collected at that time and presented diffuse reflectance spectroscopy (DRS) data that seemed to support the presence of Al-substituted Ni-LDH. Scheinost et al. (14) summarized the shortcomings of EXAFS. The Ni–O and Ni–Ni atomic distances derived from EXAFS could not uniquely identify the precipitate structure. In addition, the coordination number was deemed insufficiently precise to determine the presence or absence of Al and Si. Using DRS data, Scheinost et al. (14) were able to show a clear shift of ν_2 peak positions in spectra from synthetic Ni–Al LDH and α -Ni(OH)₂ standards. The ν_2 peak positions for Ni-precipitates on pyrophyllite and gibbsite fit that of Ni–Al LDH, and the precipitates on silica and talc fit that of α -Ni(OH)₂. Scheinost and Sparks (17) revisited the EXAFS data and determined that the beat pattern in the 8 Å⁻¹ region contained oscillations characteristic of Al-for-Ni substitutions. This corroborated the DRS findings. Finally, wavelet analysis was applied to EXAFS data to demonstrate the presence of Al in the first and third metal shells (18, 20).

The AEM data in this study also support the presence of Al in approximately 20% of the octahedral sites. Since Al is mobile under the electron beam, this is likely a minimum Al content. Aluminum mobility also explains the fact that the precipitate transforms to the bunsenite structure (Al-free) during beam damage.

Although the EXAFS data indicate that the local structure of the Ni is the Ni,Al-LDH phase, the TEM data show that the precipitate is amorphous and would more appropriately be labeled α -Ni,Al-LDH. This result is not achievable with the EXAFS technique which is limited to probe the local structure up to a radius of 0.5 to 1.0. Waychunas (21) outlined various XAS methods to gather information beyond this range—both with enthusiasm and caution. However, the simplicity of interpretation of HRTEM images (once beam-induced artifacts are eliminated) behooves the use of both techniques for a more complete characterization of nanosized or poorly crystalline materials.

Thompson (8, 22) synthesized Co,Al-LDH in bulk and as precipitates on kaolinite. Both PXRD and TEM analysis showed that their precipitates were crystalline (2–10 nm). In addition, the Ni,Al-LDH synthesized by Peltier (12) was also crystalline. Therefore, it is not the case that transition metal LDH phases are necessarily amorphous, but that in

some circumstances the precipitates fail to nucleate nanocrystals. The reasons for this are unclear. However, Si concentrations of about 0.5 mmol/L have been observed in similar systems (23, 24). These Si concentrations may influence LDH nucleation in several ways, including preferential formation of metal-hosting silicates, the interlayer silication of LDH, and a growth inhibition of LDH, explaining the amorphous state of the observed LDH.

The previous studies of α -Ni-Al LDH demonstrated that its dissolution stability increased with age (10–12, 25). Two hypotheses were presented: (1) crystal sizes increased, (2) there was a silication of the LDH interlayer space, which could be interpreted as formation of a Ni–Al layer silicate precursor. Since the precipitates were amorphous, even after 5 years in the reaction vessel, hypothesis 1 is not valid for this set of samples. However, there could be a decrease in the porosity and surface area of the precipitate over time. Analytical TEM data cannot shed light on hypothesis 2 since an assumption of the AEM data analysis was that the precipitate is Si free. However, if the precipitates did contain Si, the Si:Al value would be higher, and thus, the amount of Al in the precipitate would be underestimated.

The emphasis on the amorphous state of the material may seem purely semantic. However, nearly all physical properties of amorphous materials (AM) differ greatly from those of their crystalline counterparts. One important property is the solubility of the material. For example, the solubility of amorphous silica is much greater than quartz in water ((26) and references within). The surface area of an AM is difficult to define since there are no means to measure it by X-rays. There are essentially no coherent X-ray scattering domains. An amorphous particle could have any dimension, and yet, produce the same X-ray profile. Surface area could be determined by BET methods, but only in simple monophase samples and not complex mixtures as in natural samples. For natural soil samples, only by direct observation in the TEM could the extent and texture of the amorphous particles be defined. However, the porosity and available surface area of AM is still important.

The crystalline nature of materials tends to restrict the compositional ranges due to its limited number of bonding environments. Amorphous materials have more relaxed restrictions, although little is known about the compositional ranges of naturally occurring AM. The ability of an AM to adsorb or absorb elements is likely to be different from that of their crystalline analogs. Although we have no data to support this notion, the high probability of increased nanoscale porosity and permeability relative to more dense crystalline phases makes AM a good candidate for environmental “sponges”.

Although naturally occurring AM is likely to be an important constituent of environmental samples, it is difficult to detect by routine analysis. However, PXRD methods have been developed to quantify the amounts of AM in complicated mixtures of Earth materials (27, 28). Even in the TEM, the sharp peaks in SAED patterns of crystalline substances tend to overshadow AM diffraction which lies in the background. In complicated natural samples, small amounts of AM will undoubtedly go undetected, but could coat the surfaces of all the crystalline phases present. In this case, the undetected AM could govern the reactions with environmental fluids, while our bias toward crystalline phases would lead us to erroneous conclusions as to what is important. Here, by careful examination of environmental particle surfaces by TEM or other surface techniques (e.g., Auger, XPS) the elusive AM could be characterized.

The importance of AM in the environment has probably been underestimated due to its lack of detection. It is likely that future studies focusing on AM will prove that AM is more prevalent than currently thought.

Acknowledgments

We thank Harald Funke (FZD) for help with the EXAFS wavelet analysis. The manuscript was greatly improved by comments from Helge Stanjek, Ruben Kretzschmar, and two anonymous reviewers. All electron microscopy was done at the High-Resolution Analytical Electron Microscopy facility at Johns Hopkins University which was obtained in part from grants from the Keck Foundation and NSF.

Supporting Information Available

Information related to EXAFS and beam damage investigation of the 5-year sample. This information is available free of charge via the Internet at <http://pubs.acs.org>.

Literature Cited

- (1) Chisholm-Brause, C. J.; O'Day, P. A., Jr.; Parks, G. A. Evidence for the multinuclear metal-ion complexes at solid-solution interfaces from x-ray absorption spectroscopy. *Nature* **1990**, *348*, 528–530.
- (2) d'Espinose de la Caillerie, J.-B.; Kermarec, M.; Clause, O. Impregnation of γ -alumina with Ni(II) and Co(II) at neutral pH: Hydrotalcite-type coprecipitate formation and characterization. *J. Am. Chem. Soc.* **1995**, *117*, 11471–11481.
- (3) McNear, D. H.; Chaney, R. L.; Sparks, D. L. The effects of soil type and chemical treatment on nickel speciation in refinery enriched soils: A multi-technique investigation. *Geochim. Cosmochim. Acta* **2007**, *71*, 2190–2208.
- (4) Nachtegaal, M.; Marcus, M. A.; Sonke, J. E.; Vangronsveld, J.; Livi, K. J. T.; Van der Lelie, D.; Sparks, D. L. Effects of in situ remediation on the speciation and bioavailability of zinc in a smelter contaminated soil. *Geochim. Cosmochim. Acta* **2005**, *69*, 4649–4664.
- (5) Scheidegger, A. M.; Lamble, G. M.; Sparks, D. L. Spectroscopic evidence for the formation of mixed-cation hydroxide phases upon metal sorption on clays and aluminum oxides. *J. Colloid Interface Sci.* **1997**, *186*, 118–128.
- (6) Scheidegger, A. M.; Strawn, D. G.; Lamble, G. M.; Sparks, D. L. The kinetics of mixed Ni-Al hydroxide formation on clay and aluminum oxide minerals: A time-resolved XAFS study. *Geochim. Cosmochim. Acta* **1998**, *62*, 2233–2245.
- (7) Towle, S. N.; Bargar, J.; Brown, G. E.; Parks, G. A. Surface precipitation of Co(II) (aq) on Al_2O_3 . *J. Colloid Interface Sci.* **1997**, *187*, 62–82.
- (8) Thompson, H. A.; Parks, G. A.; Brown, G. E., Jr. Dynamic interactions of dissolution, surface adsorption, and precipitation in an aging cobalt(II)-clay-water system. *Geochim. Cosmochim. Acta* **1999**, *63*, 1767–1779.
- (9) Everhart, J. L.; McNear, D.; Peltier, E.; van der Lelie, D.; Chaney, R. L.; Sparks, D. L. Assessing nickel bioavailability in smelter-contaminated soils. *Sci. Total Environ.* **2006**, *367*, 732–744.
- (10) Scheckel, K. G.; Scheinost, A. C.; Ford, R. G.; Sparks, D. L. Stability of layered Ni hydroxide surface precipitates - A dissolution kinetics study. *Geochim. Cosmochim. Acta* **2000**, *64*, 2727–2735.
- (11) Scheckel, K. G.; Sparks, D. L. Kinetics of the formation and dissolution of Ni precipitates in a gibbsite/amorphous silica mixture. *J. Colloid Interface Sci.* **2000**, *229*, 222–229.
- (12) Peltier, E.; Allada, R.; Navrotsky, A.; Sparks, D. L. Nickel solubility and precipitation in soils: a thermodynamic study. *Clays Clay Min.* **2006**, *54*, 153–163.
- (13) Gräfe, M.; Tappero, R. V.; Marcus, M. A.; Sparks, D. L. Arsenic speciation in multiple metal environments: II. Microspectroscopic investigation of CCA contaminated soil. *J. Colloid Interface Sci.* **2008**, *321*, 1–20.
- (14) Scheinost, A. C.; Ford, R. G.; Sparks, D. L. The role of Al in the formation of secondary Ni precipitates on pyrophyllite, gibbsite, talc, and amorphous silica: A DRS study. *Geochem. Cosmochim. Acta* **1999**, *63*, 3193–3203.
- (15) Scheidegger, A. M.; Fendorf, M.; Sparks, D. L. Mechanisms of nickel sorption on pyrophyllite: Macroscopic and microscopic approaches. *Soil Sci. Soc. J.* **1996**, *60*, 1763–1772.
- (16) Bright, D. S. MacLispix: A special purpose public domain image analysis program for the Macintosh. *Microbeam Anal.* **1995**, *4*, 151–163.
- (17) Scheinost, A. C.; Sparks, D. L. Formation of layered single and double metal hydroxide precipitates at the mineral/water interface: A multiple scattering XAFS analysis. *J. Colloid Interface Sci.* **2000**, *223*, 167–178.
- (18) Funke, H.; Scheinost, A. C.; Chukalina, M. Wavelet analysis of extended X-ray absorption fine structure data. *Phys. Rev., B* **2005**, *71*, 094110.
- (19) van Aken, P. A.; Langenhorst, F. Nanocrystalline, porous periclase aggregates as product of brucite dehydration. *Eur. J. Miner.* **2001**, *13*, 329–341.
- (20) Funke, H.; Chukalina, M.; Scheinost, A. C. A new FEFF-based wavelet for EXAFS data analysis. *J. Synchrotron Radiat.* **2007**, *14*, 426–432.
- (21) Waychunas, G. A. Structure, aggregation and characterization of nanoparticles. In *Nanoparticles and the Environment*; Banfield, J. F., Navrotsky, A., Eds.; Reviews in Mineralogy and Geochemistry, vol. 44; Mineralogical Society of America: Washington, DC, 2001; pp 105–166.
- (22) Thompson, H. A.; Parks, G. A.; Brown, G. E., Jr. Formation and release of cobalt(II) sorption and precipitation products in aging kaolinite-water slurries. *J. Colloid Interface Sci.* **2000**, *222*, 241–253.
- (23) Voegelin, A.; Scheinost, A. C.; Buhmann, K.; Barmettler, K.; Kretzschmar, R. Slow formation and dissolution of Zn precipitates in soil: A combined column-transport and XAFS study. *Environ. Sci. Technol.* **2002**, *36*, 3749–3754.
- (24) Voegelin, A.; Pfister, S.; Scheinost, A. C.; Marcus, M. A.; Kretzschmar, R. Changes in zinc speciation in field soil after contamination with zinc oxide. *Environ. Sci. Technol.* **2005**, *39*, 6616–6623.
- (25) Ford, R. G.; Scheinost, A. C.; Sheckel, K. G.; Sparks, D. L. The link between clay mineral weathering and the stabilization of Ni surface precipitates. *Environ. Sci. Technol.* **1999**, *33*, 3140–3144.
- (26) Fournier, R. O.; Rowe, J. J. The solubility of amorphous silica in water at high temperatures and high pressures. *Am. Mineral.* **1977**, *62*, 1052–1056.
- (27) Chipera, S. J.; Bish, D. L. FULLPAT: A full-pattern quantitative analysis program for X-ray powder diffraction using measured and calculated patterns. *J. Appl. Crystallogr.* **2002**, *35*, 744–749.
- (28) Rancourt, D. G.; Dang, M.-Z. Absolute quantification by powder X-ray diffraction of complex mixtures of crystalline and amorphous phases for applications in the Earth sciences. *Am. Mineral.* **2005**, *90*, 1571–1586.

ES8015606